

# iGSE- $C_D$ —An Electric-/Displacement-Field Related Steinmetz Model for Class II Multilayer Ceramic Capacitors Under Low-Frequency Large-Signal Excitation

DAVID MENZI <sup>1</sup> (Member, IEEE), MORRIS HELLER <sup>1</sup> (Student Member, IEEE), GEORGE KERRIDGE <sup>2</sup>, PETER MARLEY<sup>2</sup>, ANGELA ELLMORE<sup>2</sup>, SHMUEL BEN-YAAKOV <sup>3</sup> (Life Fellow, IEEE), AND JOHANN W. KOLAR <sup>1</sup> (Fellow, IEEE)

<sup>1</sup>Power Electronics Systems Laboratory, ETH Zurich, 8092 Zurich, Switzerland

<sup>2</sup>Knowles Precision Devices, Norwich NR14 8FB, U.K.

<sup>3</sup>Ben-Gurion University of the Negev, Beer-Sheva 84105, Israel

CORRESPONDING AUTHOR: DAVID MENZI (e-mail: menzi@lem.ee.ethz.ch)

**ABSTRACT** Multilayer Ceramic Capacitors (MLCCs) are of paramount importance in electronics and ferroelectric Class II dielectrics enable outstanding energy-density values. However, the non-linear dielectric constant and associated low-frequency large-signal excitation losses of Class II MLCCs may cause critical overheating. A peak-charge based Steinmetz loss model entitled iGSE- $C_Q$  is known in literature and allows to accurately calculate MLCC low-frequency large-signal excitation losses under various operating conditions including biased and non-sinusoidal excitation voltage waveforms. Such a macroscopic iGSE- $C_Q$  model, however, is inherently limited to a specific MLCC, and in contrast to Steinmetz loss modeling for ferromagnetic inductor cores, the losses of other devices employing the same dielectric material cannot be predicted. Recent literature therefore proposed a microscopic and/or material specific MLCC Steinmetz Model entitled iGSE- $C_D$  which allows to calculate the losses of any MLCC of the same dielectric material based upon just a single set of Steinmetz parameters. However, due to the lack of information on the internal device geometry, the iGSE- $C_D$  could be verified only indirectly so far by means of a loss normalization based on the device capacitance and rated voltage. In this paper, we demonstrate the feasibility of a microscopic iGSE- $C_D$  MLCC loss model enabled by manufacturer data on the internal capacitor structure. The iGSE- $C_D$  is verified for two different MLCC series employing a conventional X7R dielectric and a novel Hiteca (with reduced non-linearity) Class II dielectric material with loss estimation error below 22%. This error results due to component tolerances and is acceptable, especially when compared to the loss calculation based on the datasheet information which can be off by up to a factor of ten. The analysis of the Hiteca dielectric reveals a frequency behavior different to the X7R material, and is discussed in the Appendix of this paper.

**INDEX TERMS** Multilayer ceramic capacitor, MLCC, loss modeling, Steinmetz Equation, iGSE, iGSE-C, DC-AC power converters, AC-DC power converters, inverters, rectifiers, power capacitors.

## I. INTRODUCTION

Multilayer Ceramic Capacitors (MLCCs) are a foundation of electronics [1], and Class II MLCCs with ferroelectric dielectrics enable ultra-high energy densities [1], [2], [3]. This, however, comes at the cost of a non-linear dielectric constant and Fig. 1 depicts an exemplary small-signal /

differential capacitance  $C_d$  over dc bias voltage  $U_{dc}$  curve of a Class II X7R MLCC (the material code X7R indicates the tolerable minimum and maximum device temperatures [−55 °C to 125 °C], as well as the associated change of capacitance of ±15% [1]). Here the differential capacitance  $C_d$  reduces drastically with increasing bias voltage and drops

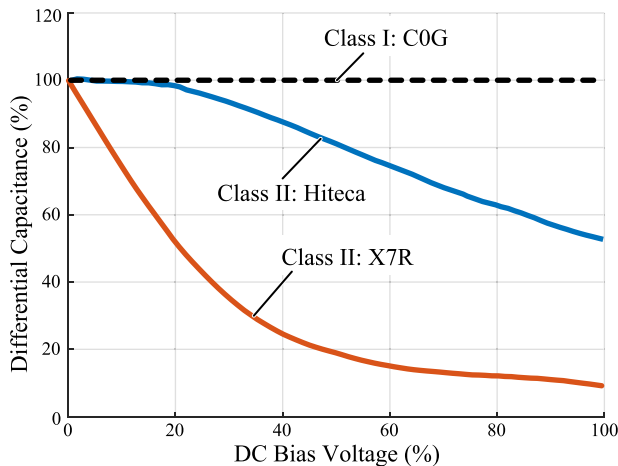


**FIGURE 1.** Exemplary small-signal / differential capacitance  $C_d$  (normalized to the nominal capacitance value  $C_0$  at zero dc bias) over dc-bias voltage  $U_{dc}$  (normalized by the capacitor rated voltage  $U_R$ ) of a ferroelectric Class II (X7R) MLCC, a new Hiteca MLCC with reduced capacitance variation, and – for comparison – a low-energy-density Class I (C0G) MLCC.

below 20% of the nominal / unbiased capacitance value  $C_0$ . For comparison, Fig. 1 also depicts a Class I C0G MLCC with a constant capacitance value, as well as a new Class II Hiteca<sup>1</sup> MLCC from Knowles [4], [5] with reduced capacitance non-linearity over bias voltage.

This non-linear dielectric constant of Class II MLCCs is accompanied by substantial low-frequency large-signal excitation losses which are reported in literature [6], [7], [8], [9] and may lead to critical device overheating even in the range of 100 Hz excitation frequency which is present in, e.g., active power pulsation buffers for single-phase Power Factor Correction (PFC) rectifiers or motor drive sinewave filters. It is well known that a simple Effective Series Resistance (ESR) loss model cannot capture the non-linear loss behavior of MLCCs [10], and Class II MLCC dissipation factors can increase tenfold under large-signal excitation compared to the datasheet performance observed under small-signal excitation [9].

Based upon the duality of ferromagnetic core materials (used for inductors and transformers) and ferroelectric dielectric materials [11], a peak-charge-excitation-based MLCC Steinmetz loss model was introduced in [9]: The losses were found to scale according to a power law relationship with the MLCC charge amplitude and excitation frequency, and a set of Steinmetz parameters allows to accurately calculate the low-frequency large-signal excitation losses. The model was shown to hold for dc-biased excitation and further extended to non-sinusoidal voltage excitation, and thus, named improved Generalized Steinmetz Equation for ceramic Capacitors (iGSE- $C_Q$ ) [9].

The iGSE- $C_Q$  model, however, is limited to a specific MLCC, and in contrast to Steinmetz magnetic loss modeling,

the losses of other devices employing the same dielectric material with different rated voltage and/or different nominal capacitance value cannot be predicted.

As highlighted in [12], this limitation of the iGSE- $C_Q$  results as the model bases on the macroscopic device behavior (i.e., on the overall peak device charge  $Q_{pk}$  and voltage  $U_{pk}$ ). In contrast, Steinmetz modeling for magnetic losses is conducted on a microscopic level: The loss *density* of a magnetic core is calculated based on the B-field excitation, such that a single set of Steinmetz parameters allows to calculate the losses of a ferromagnetic material for various core geometries.

Accordingly, Ref. [12] proposed a *microscopic* peak D-field-excitation-based loss model named iGSEC<sub>D</sub> which is – similar to ferromagnetic loss modeling – applicable to MLCCs of the same dielectric material across rated voltage and nominal capacitance. However, due to the lack of information on the internal structure of commercially available MLCCs the iGSEC<sub>D</sub> could be verified (up to now) only indirectly by means of a loss normalization based on the device capacitance and rated voltage [12].

In this paper, based on manufacturer data on the internal MLCC structures we verify the iGSEC<sub>D</sub> model and demonstrate loss calculations for several devices employing the same dielectric material for both Class II X7R and new Hiteca MLCCs.

The paper is structured as follows: Section I provides the relevant theoretical background for the macroscopic and microscopic MLCC loss modeling. Section II presents experimental results validating the iGSEC<sub>D</sub> and a detailed discussion of the findings. Then, Section III discusses the applicability of the iGSEC<sub>D</sub> and includes an exemplary design process. Section IV summarizes the main findings and indicates paths for future research and Appendix A provides additional information on the frequency behavior of Hiteca MLCCs.

## I. MICROSCOPIC MLCC STEINMETZ MODELING

In this section, in a first step, the relationship of microscopic and macroscopic MLCC quantities is summarized. Then, the associated loss models are introduced and the conversion of macroscopic to microscopic Steinmetz parameters is discussed.

### A. MICROSCOPIC MLCC PROPERTIES

Fig. 2(a) presents the voltage-charge  $U - Q$  hysteresis loop of an X7R MLCC (2220Y5000105KXTWS2 from Knowles, designated as  $C_5$  in Table 1). Here, the energy  $W$  dissipated within one cycle (or the losses  $P$  resulting by multiplication of  $W$  with the excitation frequency  $f$ ) is defined with

$$W = \int u dq = \frac{P}{f}, \quad (1)$$

and corresponds to the area enclosed by the  $U - Q$  hysteresis loop. As mentioned, the measured loss  $P$  is device-specific and cannot be used directly to calculate the losses for the same operating point resulting in another device of the same

<sup>1</sup>Hiteca is a registered trademark by Knowles.

TABLE 1. Typical Geometry Information of the Considered MLCCs From Knowles<sup>1</sup>

Part Number	Diell. Mat.	Design.	$U_R$ (V)	$C_0$ (nF)	$t$ ( $\mu\text{m}$ )	$A$ ( $\text{mm}^2$ )	$V_{\text{diel}}$ ( $\text{mm}^3$ )	$k_Q$	$\alpha$	$\beta$
1812Y5000104KXT	X7R	$C_1$	500	100	36	178	6.4	1.5e+07	1.0	2.2
1812Y5000274KXT	X7R	$C_2$	500	270	35	471	16.4	3.7e+06	1.0	2.2
2220Y5000334KXT	X7R	$C_3$	500	330	35	590	20.6	3.4e+06	1.0	2.2
2220Y5000564KXT	X7R	$C_4$	500	560	35	990	34.5	1.0e+06	1.0	2.1
2220Y5000105KXTWS2	X7R	$C_5$	500	1000	33	1649	54.7	4.8e+05	1.0	2.1
2220Y6300105KXTWS2	X7R	$C_6$	630	1000	33	1649	54.7	7.0e+05	1.0	2.2
1812Y1K00104KXT	X7R	$C_7$	1000	100	52	274	14.4	5.0e+06	1.0	2.1
2220Y1K00104KXT	X7R	$C_8$	1000	100	60	308	18.4	1.1e+07	1.0	2.2
1812Y1K00154KXTWS2	X7R	$C_9$	1000	150	45	345	15.4	2.6e+06	1.0	2.1
2220Y1K00474KXTWS2	X7R	$C_{10}$	1000	470	46	1127	51.8	1.3e+06	1.0	2.1
2220Y1K00474KXTWS3	X7R	$C_{11}$	1000	470	46	1127	51.8	1.4e+06	1.0	2.2
2225Y5000474KZT	Hiteca	$C_{12}$	500	470	40	1808	72.1	6.0e+03	1.5	2.1
2225Y9000184KZT	Hiteca	$C_{13}$	900	180	69	1188	81.7	3.8e+03	1.7	2.0

<sup>1</sup>Terminology: rated voltage  $U_R$ , nominal (un-biased) capacitance value  $C_0$ , dielectric layer thickness  $t$ , total active area  $A$ , dielectric volume  $V_{\text{diel}}$ , macroscopic Steinmetz parameters  $k_Q, \alpha, \beta$ .

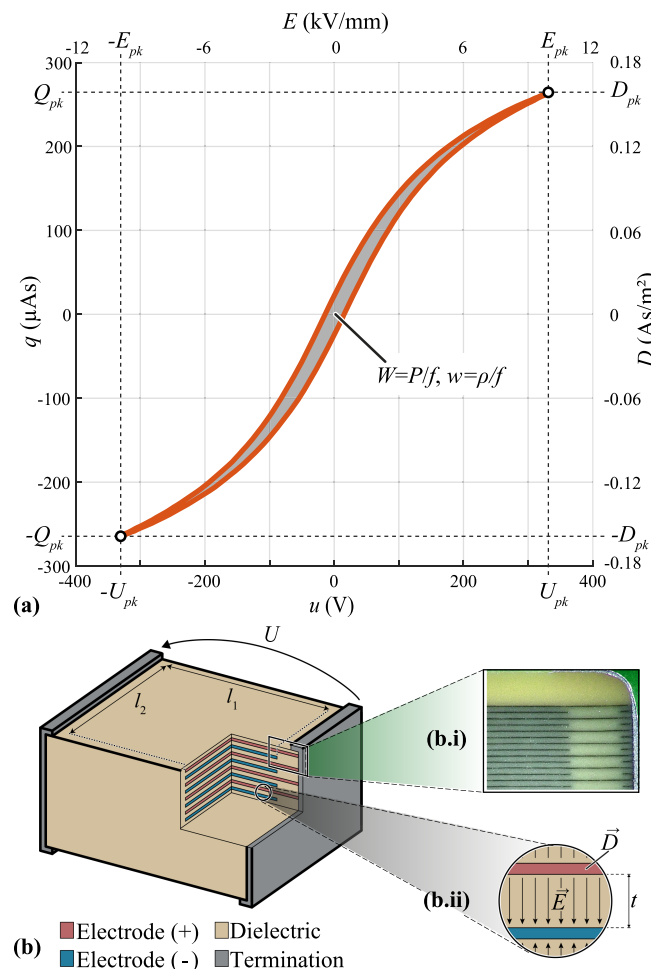


FIGURE 2. (a) Measured voltage-charge  $U - Q$  (or microscopic electric-displacement field  $E - D$ ) hysteresis loop of an X7R MLCC (2220Y5000105KXTWS2 designated as  $C_5$  in Table 1). The MLCC is excited to a peak voltage of  $U_{pk} = 330$  V at a frequency  $f = 100$  Hz and the enclosed hysteresis area corresponds to the energy  $W$  (or microscopically to the energy density  $w$  in a unit volume of the dielectric) dissipated within one cycle. (b) illustration of the internal structure of an MLCC: (b.i) cross-section view of a commercial MLCC, and (b.ii) microscopic field quantities in between two MLCC layers.

dielectric material but with different voltage rating or different nominal capacitance value.

This limitation can be resolved, if instead of the macroscopic device behavior, i.e., the MLCC voltage  $U$  and charge  $Q$ , the *microscopic* dielectric material properties based upon the electric field  $E$  and the displacement field  $D$  are considered [12]. Ferroelectric materials have spontaneous polarization, where a dipole is created due to the slight displacement of an atom from the center of a crystal structure. In  $\text{BaTiO}_3$ , the most common material for Class II dielectrics, the Ti atom is displaced off the central position within the  $\text{Ti-O}_6$  polyhedra producing the effective dipole. At the microscopic level the material contains ‘domains’ of orientated dipoles, but at the macroscopic level the net polarization is zero (for an un-poled material). When an electric field is applied, these domains will be influenced to polarize in the direction of the external field. Some domains will align (by random chance) to the electric field, where they will begin to grow and coalesce. ‘Domain wall motion’ is often used to explain the work required to make domains grow/shrink. This is also used to explain the dielectric dissipation energy density  $w$  (or power loss density  $\rho$ ), which is – for a certain  $E$ -field excitation – identical for all devices of the same dielectric material.

The local dissipation energy density  $w$  (or the power loss density  $\rho$  resulting by multiplication of  $w$  with the excitation frequency  $f$ ) is defined with

$$w = \int E dD = \frac{\rho}{f}, \quad (2)$$

and corresponds to the area enclosed by the  $E - D$  hysteresis loop in Fig. 2(a).

Fig. 2(b) illustrates the internal structure of an MLCC which represents an ideal plate capacitor in good approximation and hence a homogeneous field distribution is assumed in the following. The MLCC comprises  $N$  dielectric layers enclosed by  $N + 1$  electrodes of alternating polarity (the coloring of the positive and negative electrodes does not indicate a different material but serves to highlight the electrode potential). As highlighted in Fig. 2(b.ii) the full terminal voltage  $U$

is applied across each dielectric layer of thickness  $t$ , resulting in an  $E$ -field

$$E = U/t, \quad (3)$$

and a parallel connection of the  $N$  dielectric layers.

The electrodes comprise a certain margin towards the termination of opposing polarity and towards the MLCC edge, such that each MLCC layer comprises an (active) overlap area  $A_N = l_1 \cdot l_2$  (see Fig. 2(b)). Hence, the macroscopic device charge  $Q$  is spread across the total active area  $A = N \cdot A_N$  resulting in a  $D$ -field

$$D = Q/A. \quad (4)$$

Last, the MLCC loss density  $\rho$  results when dividing the device losses  $P$  by the total active dielectric volume  $V_{\text{diel}} = A \cdot t$  with

$$\rho = \frac{P}{V_{\text{diel}}} = \frac{P}{A \cdot t}. \quad (5)$$

In summary, the relation between the macroscopic MLCC electric quantities, i.e., voltage  $U$ , charge  $Q$  and losses  $P$ , and the microscopic MLCC electric quantities, i.e.,  $E$ -field,  $D$ -field and loss density  $\rho$ , is defined by the MLCC geometrical properties, i.e., effective dielectric layer thickness  $t$  and total active area  $A$ , such that the macroscopic device behavior can be described based upon the fundamental / microscopic material properties and vice versa.

Table 1 lists the commercially available MLCCs considered in this publication with the typical geometrical properties provided by the manufacturer. For the MLCC highlighted in Fig. 2(a) ( $C_5$  in Table 1), the excitation voltage amplitude of  $U_{\text{pk}} = 330 \text{ V}_{\text{pk}}$  corresponds with (3) to  $E_{\text{pk}} = 10 \text{ kV/mm}$ , and the resulting peak charge  $Q_{\text{pk}} = 260 \text{ }\mu\text{C}$  corresponds with (4) to  $D_{\text{pk}} = 0.16 \text{ As/m}^2$ .

## B. CONSIDERED LOSS MODELS

According to the device-specific Steinmetz model from [9] Class II MLCC large-signal excitation losses  $P$  scale according to a power-law relationship with the peak charge  $Q_{\text{pk}}$  and the excitation frequency  $f$  as

$$P = W \cdot f = k_Q \cdot f^\alpha \cdot Q_{\text{pk}}^\beta, \quad (6)$$

with the Steinmetz parameters  $k_Q, \alpha, \beta$ . In case of non-sinusoidal excitation waveforms (e.g., third-harmonic injection in a motor drive inverter), the losses can be derived as

$$P = \frac{1}{T} \int_0^T k_i \left| \frac{dQ}{dt} \right|^\alpha (\Delta Q)^{\beta-\alpha} dt, \quad (7)$$

which is entitled as the improved Generalized Steinmetz Equation for ceramic Capacitors (iGSE-C<sub>Q</sub>) [9], [13], with the peak-to-peak charge excitation  $\Delta Q = 2 \cdot Q_{\text{pk}}$ , and  $k_i$  defined by the Steinmetz parameters according to [13] as

$$k_i = \frac{k}{(2\pi)^{\alpha-1} \int_0^{2\pi} |\cos \theta|^\alpha 2^{\beta-\alpha} d\theta}. \quad (8)$$

The iGSE-C<sub>Q</sub> considers the instantaneous MLCC losses as a function of the instantaneous change in charge  $dQ/dt$  and the overall peak-to-peak charge excitation  $\Delta Q$ . In case of non-monotonic excitation waveforms, major-minor loop splitting is performed with  $\Delta Q$  in (7) equal to the excitation of the respective loop as highlighted in [9], [13]. Note that for  $\alpha \approx 1$  (as found in [9] for the considered X7R MLCC), (7) collapses to (6). Hence, for  $\alpha \approx 1$ , (6) allows to calculate MLCC losses for non-sinusoidal waveforms when minor/major loop splitting is applied. Therefore, in the following both (6) and (7) are referred to as an iGSE-C<sub>Q</sub> model.

In contrast to device specific models, according to the material-specific iGSEC<sub>D</sub> model [12] the *microscopic* power loss density  $\rho$  (and the dissipation energy density  $w$ ) scale according to a power-law relationship with the peak D-field  $D_{\text{pk}}$  and the excitation frequency  $f$  as

$$\rho = w \cdot f = k_D \cdot f^\alpha \cdot D_{\text{pk}}^\beta, \quad (9)$$

with the Steinmetz dielectric material parameters  $k_D, \alpha, \beta$ . For non-sinusoidal excitation the loss density is derived based on

$$\rho = \frac{1}{T} \int_0^T k_{i,D} \left| \frac{dD}{dt} \right|^\alpha (\Delta D)^{\beta-\alpha} dt, \quad (10)$$

with the peak-to-peak displacement field  $\Delta D = 2 \cdot D_{\text{pk}}$ , and  $k_{i,D}$  derived from (8) by substituting  $k$  with  $k_D$ .

Combining now (6) and (9) with (5), the material-specific iGSEC<sub>D</sub> parameter  $k_D$  can be derived from the device-specific iGSE-C<sub>Q</sub> parameter  $k_Q$  with [12]

$$k_D = \frac{k_Q}{V_{\text{diel}}} \left( \frac{Q_{\text{pk}}}{D_{\text{pk}}} \right)^\beta = \frac{k_Q}{V_{\text{diel}}} A^\beta, \quad (11)$$

whereas  $\alpha$  and  $\beta$  are identical for both the iGSE-C<sub>Q</sub> and the iGSEC<sub>D</sub>. Hence, the loss characterization and the geometry information of a single MLCC is sufficient to characterize the dielectric material and/or parameterize the iGSEC<sub>D</sub> model, which advantageously applies to all MLCCs employing the same material.

## II. EXPERIMENTAL VERIFICATION

Results obtained with an automated Sawyer-Tower setup (for more details on the setup we refer to [12]) for the MLCCs listed in Table 1 are presented in Fig. 3. The scatter points represent measurement points (round symbols for X7R and triangular for Hiteca dielectrics) and an excitation frequency of  $f = 100 \text{ Hz}$  is considered here.

As can be observed in Fig. 3(a.i), the relationship between the MLCC peak-charge  $Q_{\text{pk}}$  and the peak voltage  $U_{\text{pk}}$  is non-linear and fundamentally different across the considered devices. If the macroscopic MLCC peak charge and voltage values are translated into the corresponding microscopic quantities with (3), (4) and the typical geometrical dimensions in Table 1, the plot in Fig. 3(a.ii) results. There, the peak displacement field  $D_{\text{pk}}$  vs. peak electric field  $E_{\text{pk}}$  behavior is almost identical for all considered devices of the same

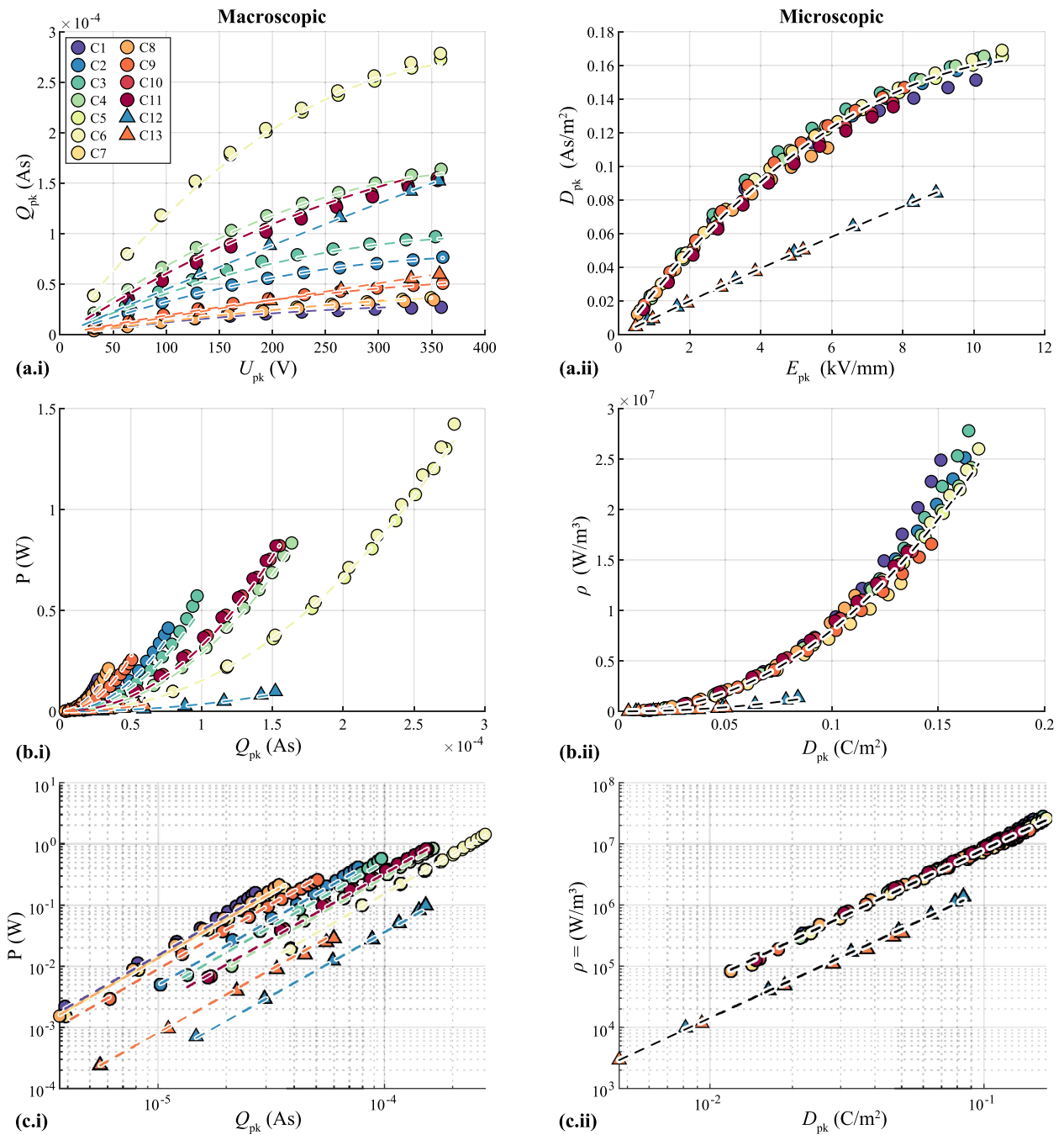


**FIGURE 3.** Experimental results across increasing voltage amplitude for a constant excitation frequency  $f = 100$  Hz for the devices stated in Table 1 with X7R (round scatter symbols) and Hiteca dielectrics (triangular scatter symbols): (a.i) non-linear MLCC peak-charge  $Q_{pk}$  vs. peak voltage  $U_{pk}$  and (a.ii) peak displacement field  $D_{pk}$  vs. peak electric field  $E_{pk}$ . (b.i) MLCC losses  $P$  vs. peak-charge  $Q_{pk}$  and (b.ii) dielectric loss density  $\rho$  vs. peak displacement field  $D_{pk}$  in a linear scale. (c.i) MLCC losses  $P$  vs. peak-charge  $Q_{pk}$  and (c.ii) dielectric loss density  $\rho$  vs. peak displacement field  $D_{pk}$  in a logarithmic scale. The dashed lines in the plots related to the microscopic MLCC properties (i.e., a.ii, b.ii, c.ii) represent the associated fits / models describing the microscopic dielectric material properties according to Table 2. The dashed lines in the plots related to the macroscopic MLCC properties (i.e., a.i, b.i, c.i) are also obtained based upon the microscopic dielectric material properties and are scaled according to the geometrical dimensions of the MLCCs in Table 1 with (3)–(5).

dielectric material. In fact a simple second order polynomial fit (dashed line in Fig. 3(a.ii)) for the relationship

$$D_{pk}(E_{pk}) = k_1 \cdot E_{pk} + k_2 \cdot E_{pk}^2 \quad (12)$$

with the parameters according to Table 2 results in a  $D$ -field fitting error below 10% for the maximum excitation values of the considered devices. Further, Fig. 3(a.ii) clearly illustrates the reduced non-linearity of the Hiteca dielectric compared

**TABLE 2. Material Specific Steinmetz Parameters (Extracted From  $C_5$  and  $C_{12}$ )**

Diel. Mat.	$k_1$ [As/(Vm)]	$k_2$ [As/(V <sup>2</sup> )]	$k_D$	$\alpha$	$\beta$
X7R	2.8e-08	-1.1e-15	1.1e+07	1.0	2.1
Hiteca	1.0e-08	-8.8e-17	1.6e+05	1.5	2.1

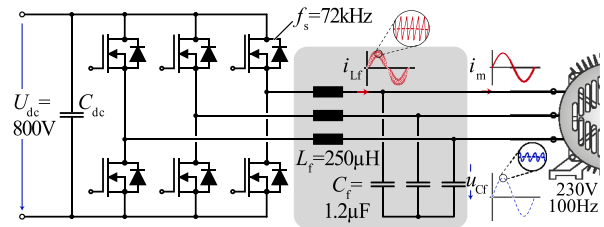
to the X7R dielectric. Note that also the dashed lines in Fig. 3(a.i) are based upon the same microscopic  $D_{pk}(E_{pk})$  characteristic (12) and scaled to macroscopic quantities according to (3), (4) and the MLCC geometry information.

Next, Fig. 3(b.i) depicts the measured MLCC losses  $P$  vs. peak-charge  $Q_{pk}$  where again MLCCs of the same dielectric may behave substantially different across excitation amplitude. The iGSE- $C_Q$  (6) allows to describe the loss-charge relationship of each device individually across excitation waveform, amplitude, dc-bias and frequency [9], and Table 1 lists the obtained Steinmetz parameters for each considered device. However, as mentioned, a new MLCC of the same dielectric material would need to be measured first to obtain its device-specific iGSE- $C_Q$  parameters, which is of course undesirable. Fig. 3(c.i) depicts the data of Fig. 3(b.i) in a logarithmic scale. There, it can be noted that a very similar slope  $\beta$  results for devices of the same dielectric material, whereas the scaling parameter  $k_Q$  is different for each device, which is in line with the consideration of Section I.

The limitation to a single device is resolved when translating the macroscopic device losses and charge of Fig. 3(b.i/c.i) into the microscopic dielectric power loss density  $\rho$  vs. peak displacement field  $D_{pk}$  in Fig. 3(c.i)/(c.ii):

The displacement field to loss relationship is now almost identical among MLCCs of the same material. The iGSEC $_D$  (9) parameters [12] are derived here with (11) from the iGSE- $C_Q$  parameters of  $C_5$  and  $C_{12}$  in Table 1 for the X7R and the Hiteca MLCCs, respectively, and stated in Table 2. The iGSEC $_D$  is represented by a black dashed line in Fig. 3(b.i)/(c.ii) and accurately describes the resulting large-signal excitation loss density at the maximum excitation amplitude with a worst-case model error of 22% for the X7R and of 16% for the Hiteca MLCCs. This deviation may result due to geometric (i.e., active area  $A$  or layer thickness  $t$ ) or also dielectric material manufacturing tolerances (for example, the nominal MLCC capacitance value is typically varying in a range of  $\pm 10\%$  or  $\pm 20\%$ ) and it is worth highlighting that a loss model error of 22% is extremely small compared to the error resulting when employing the datasheet ESR value which can be off by up to a factor of ten. The dashed lines in Fig. 3(b.i)/(c.i) are again based upon the iGSEC $_D$  and scaled to macroscopic quantities according to (3)–(5) and the MLCC geometry, and clearly illustrate the performance of the microscopic iGSEC $_D$  loss model.

Note that the Steinmetz parameters of Table 1 and Table 2 were recorded at a temperature of 25 °C (the measurement time was minimized to avoid self heating) and it is known from literature that temperature impacts the MLCC losses [7],


**FIGURE 4. Application example: a sinewave output filter of a motor drive inverter employing MLCCs reduces the high-frequency differential-mode stresses of a three-phase induction machine.**

[9] (e.g., Ref. [9] found a loss decrease of approximately 0.6%/K with increasing temperatures). Hence, similar to magnetics modeling [14], [15], future research could extend the iGSEC $_D$  model with temperature information, i.e., by providing temperature dependent Steinmetz parameters. According to literature, dielectric aging also impacts MLCC losses [16] which might also be considered. Advantageously, for the iGSEC $_D$  this can be done on a material level, i.e., with a reduced number of measurements compared to a device-specific model. Further, it would be interesting to investigate, whether the iGSEC $_D$  model is also applicable for low-voltage MLCCs (i.e., with rated voltages of up to several tens of volts) where the dielectric layer thickness is comparable to the grain size of the dielectric material, such that the assumption of a homogeneous field distribution of (3) and (4) might not be justified anymore.

Last, it is important to highlight that – in contrast to X7R MLCCs with losses increasing linearly ( $\alpha = 1.0$ ) with frequency up to  $f \approx 500$  Hz [9] – the Hiteca MLCCs show an above-linear loss increase ( $\alpha = 1.5$ ) with frequency and the frequency behavior of this material is discussed in more detail in Appendix A.

### III. DESIGN EXAMPLE

The goal of this section is to illustrate how the iGSEC $_D$  allows a straightforward MLCC selection for given converter specifications.

A motor drive sinewave output filter limiting the motor stresses as illustrated in Fig. 4 is considered here for a 3 kW induction machine with a line-to-neutral voltage of 230 V $_{rms}$  (i.e.,  $U_{pk} = 325$  V $_{pk}$ ) and a nominal stator frequency  $f = 100$  Hz (e.g., Siemens 1LE1003-1AA42-2NA4-Z H01 with 5820 rpm). The required LC-filter capacitance value is  $C_f = 1.2$   $\mu$ F and for the MLCC selection, loss and volume performance, as well as the MLCC derating (due to the non-linear capacitance value) and thermal behavior have to be considered.

In a first step, the peak E-field excitation  $E_{pk}$  of each MLCC for the considered voltage amplitude  $U_{pk} = 325$  V $_{pk}$  is calculated with (3) and the typical device thickness information in Table 1. The dielectric stresses  $E_{pk}$  are stated in Table 3 and values in a range from 4.7 kV/mm to 9.8 kV/mm result. Then, for each device the D-field is estimated with

TABLE 3. Application Example<sup>2</sup>

Design.	$U_R$ (V)	$C_0$ (nF)	$E_{pk}$ (kV/mm)	$D_{pk}$ (As/m <sup>2</sup> )	$\rho$ (W/cm <sup>2</sup> )	$\epsilon_P$ (%)	$P$ (W)	$P_{max}$ (W)	$\delta_C$ (%)	$N_{par}$	$P_{tot}$ (W)	$V_{tot}$ (cm <sup>3</sup> )
$C_1$	500	100	9.1	0.15	20.3	-10.9	0.1	0.4	24.1	50	6.4	1.8
$C_2$	500	270	9.3	0.16	20.7	-10.3	0.3	0.4	22.4	20	6.8	0.7
$C_3$	500	330	9.3	0.16	20.7	-18.4	0.4	0.9	22.4	17	7.2	2.2
$C_4$	500	560	9.3	0.16	20.7	-7.4	0.7	0.9	22.4	10	7.1	1.3
$C_5$	500	1000	9.8	0.16	21.4	-2.5	1.2	0.9	18.4	7	8.2	0.9
$C_6$	630	1000	9.8	0.16	21.4	-10.5	1.2	0.9	18.4	7	8.2	0.9
$C_7$	1000	100	6.2	0.13	13.1	13.3	0.2	0.4	48.2	25	4.7	0.9
$C_8$	1000	100	5.4	0.11	10.8	5.4	0.2	0.9	54.7	22	4.4	2.8
$C_9$	1000	150	7.3	0.14	16.0	4.9	0.2	0.4	39.5	21	5.2	0.8
$C_{10}$	1000	470	7.1	0.14	15.5	6.8	0.8	0.9	41.1	7	5.6	0.9
$C_{11}$	1000	470	7.1	0.14	15.5	7.8	0.8	0.9	41.1	7	5.6	0.9
$C_{12}$	500	470	8.1	0.08	1.0	-11.5	0.1	0.9	86.0	3	0.2	0.4
$C_{13}$	900	180	4.7	0.05	0.3	13.7	0.0	0.9	91.9	8	0.2	1.1

<sup>2</sup>Terminology: rated voltage  $U_R$ , nominal (un-biased) capacitance value  $C_0$ ; calculated peak electric  $E_{pk}$  and displacement field  $D_{pk}$ , dielectric loss density  $\rho$ , loss estimation error  $\epsilon_P$ , calculated MLCC losses  $P$ , maximum tolerable losses  $P_{max}$ , available capacitance after derating  $\delta_C$ , required number of parallel devices  $N_{par}$ , total losses  $P_{tot}$  and volume  $V_{tot}$ .

(12), allowing to calculate the MLCC loss density  $\rho$  with an error (compared to the measured values) of  $\epsilon_P < 15\%$  for all investigated devices.

The macroscopic dielectric losses  $P$  of the MLCCs are obtained by multiplying the loss density  $\rho$  with the respective dielectric volume  $V$  according to Table 1. Here it is important to highlight that the MLCC large-signal excitation losses  $P$  may lead to critical overheating and  $P_{max}$  represents the maximally tolerable device losses for the employed device packages according to [6] for a maximum temperature rise of  $\Delta T = 25$  °C. Hence,  $C_6$  and  $C_7$  cannot be employed for the considered application due to excessive self-heating with  $P > P_{max}$ .

Next, the capacitor derating with voltage (see Fig. 1) needs to be considered in order to assure the availability of the desired total capacitance of  $C_f = 1.2$   $\mu$ F and Table 3 depicts the available capacitance value  $\delta_C = C/C_0 = D'(E = E_{max})/D'(E = 0)$  which drops below 20% for some of the X7R devices. The reason for this is that the MLCCs with  $U_R = 500$  V have small layer thickness values  $t$  and in consequence large E- and D-field excitations with associated high loss-density values  $\rho$ . Hence, considering the capacitance derating  $\delta_C$  the number of required parallel devices to realize  $C_f = 1.2$   $\mu$ F is given by  $N_{par} = \frac{C_f}{\delta_C C_0}$ , allowing to calculate the overall capacitor realization losses  $P_{tot}$  and volume  $V_{tot}$  (note that  $V_{tot}$  is calculated based on the total MLCC volume and not just the dielectric volume  $V_{diel}$ ).

Among the X7R devices (i.e.,  $C_1 - C_{11}$ ) it can be stated that  $C_2$  (with rated voltage  $U_R = 500$  V) allows a very compact filter capacitor realization at the cost of high MLCC losses. In contrast,  $C_{10}$  with a rated voltage of  $U_R = 1$  kV enables lower losses (due to the elevated layer thickness  $t$ ), at the cost of a higher volume.

Within this context it is important to highlight the performance of the two considered Hiteca MLCCs  $C_{12}$  and  $C_{13}$  which feature loss density values  $\rho$  reduced by up to a factor of 60 compared to the X7R devices. Further, due to the less voltage dependent dielectric constant (see Fig. 1), the capacitance derating  $\delta_C$  is reduced, allowing to realize the  $C_f$  value

with a lower number of parallel devices  $N_{par}$  such that the overall loss and volume performance is superior compared to the considered X7R MLCCs, with a volumetrically ideal realization given by  $N_{par} = 3$  devices of  $C_{12}$ . Note that the frequency behavior of the Hiteca MLCCs (discussed in more detail in Appendix A) is fundamentally different from their X7R counterparts and hence the preferred capacitor technology is application-specification dependent.

Last, it is important to highlight that the MLCCs are – on top of the fundamental-frequency output voltage swing – subject to the time-varying high-frequency current ripple of the filter inductor current  $i_{Lf}$  (see Fig. 4) with associated high-frequency MLCCs losses. However, due to the low MLCC high-frequency ESR values, typically the MLCC high-frequency small-signal excitation losses are small compared to the low-frequency large-signal excitation losses in a sinewave filter [9]. Here, the high-frequency RMS MLCC current results to  $I_{Cf} = 1$  A<sub>rms</sub>, i.e., each of the  $N_{par} = 3$  MLCCs faces a current of 0.3 A<sub>rms</sub>, and assuming that the entire high-frequency current occurs at the switching frequency of 72 kHz, the high-frequency losses can be calculated with the measured (small-signal) ESR value of 39.5 m $\Omega$  (corresponding to a dissipation factor of 0.8%) to only 4.5 mW per device. Note that measurements available in literature indicate that some Class II MLCCs exhibit increasing ESR values with dc-bias for high-frequency small-signal excitation [17], [18], [19]. However, first, even for an ESR increase by a factor of five as found in [19], the high-frequency MLCC losses would remain extremely small, and second, measurements provided in [4] shows a low impact of the dc-bias voltage on the Hiteca MLCC high-frequency losses.

#### IV. CONCLUSION

Ferroelectric Class II Multilayer Ceramic Capacitors (MLCCs) allow extremely compact converter realizations but suffer from a non-linear capacitance value and associated substantial low-frequency large-signal excitation losses even in the 100 Hz frequency range. The ESR value commonly provided in the datasheet does not accurately describe the

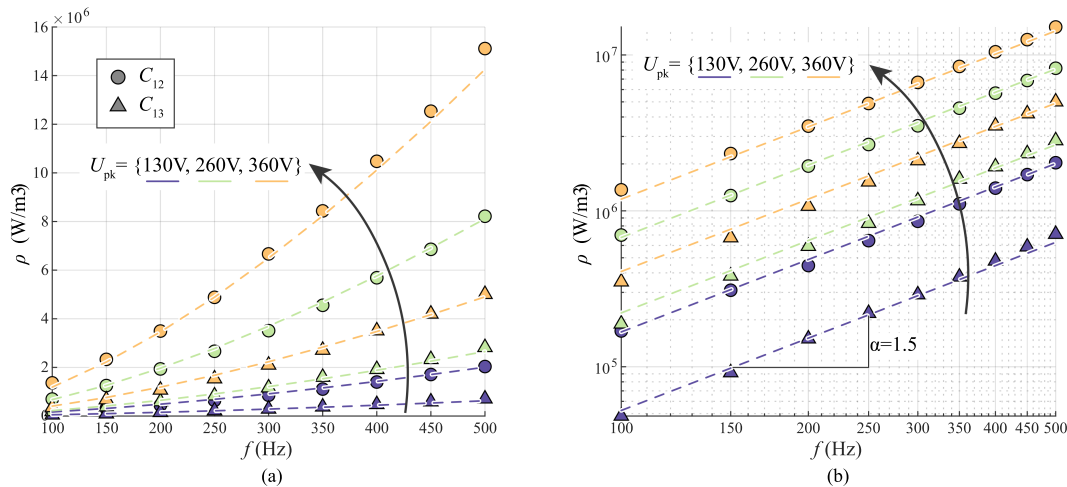


**FIGURE 5.** Loss-density  $\rho$  vs. frequency  $f$  behavior of the Hiteca MLCCs in Table 1 in (a) linear and (b) logarithmic scale. The dashed lines are obtained based upon the microscopic dielectric material properties according to Table 2 and the iGSEC $_D$  model (9).

loss behavior of such MLCCs under large-signal excitation and yields calculated losses which are off by up to a factor of ten [9]. The device-specific improved Generalized Steinmetz Equation for ceramic Capacitors (iGSE- $C_Q$ ) [9] allows to accurately calculate low-frequency large-signal excitation of ferroelectric Class II MLCCs but its Steinmetz parameters are limited to a single device, and therefore not capable of calculating the losses of a MLCCs of the same dielectric material with different rated voltage and/or different nominal capacitance.

This paper verifies the feasibility of a dielectric-material-specific and/or microscopic iGSEC $_D$  loss model [12] which allows to predict MLCC losses with an error below 22% for a large number of devices employing the same dielectric material. Hence, in the future it is sufficient to – similar to magnetics materials – thoroughly characterize commercially available dielectric materials only once. Class II MLCC low-frequency large-signal excitation losses are then calculated upon the material-specific Steinmetz parameters and information on the MLCC geometry, namely the active area  $A$  and the layer thickness  $t$ . Note that the internal MLCC structure is today not disclosed by manufacturers and the tolerances associated with these features are not known to the authors. However, one could obtain this information by means of a Scanning Electron Microscopy (SEM), an energy-dispersive X-ray spectroscopy, or a Destructive Physical Analysis (DPA) with subsequent visual inspection [20], where DPA is preferred to investigate the electrode size. Therefore, the authors hope that this information in generic form may be available upon request from MLCC manufacturers in the future, as this modeling technique becomes more important for board designers and researchers. It was further found in this publication, that for the considered application example (a motor drive inverter sinewave filter), the recently introduced Hiteca dielectric with reduced non-linearity clearly outperforms the conventional X7R Class II material.

In closing it is important to highlight again that the focus of this publication is on the low-frequency large-signal excitation Class II MLCC losses relevant for, e.g., active power pulsation buffers for single-phase PFC rectifiers or motor drive sinewave filters. Due to the high loss density values resulting under large-signal excitation the investigated frequency range is here limited to  $f \leq 500$  Hz. However, Class II MLCCs are also commonly employed as dc-link capacitors and/or find application in flying capacitor or resonant converters. There, the MLCCs are subject to dc-biased high-frequency small-signal excitation which is investigated in [17], [18], [19]. Currently ongoing research [21] successfully employs the Steinmetz models of [9], [12] for dc-biased high-frequency small-signal excitation with frequencies up to 200 kHz.

## APPENDIX A LOSS-FREQUENCY BEHAVIOR OF HITECA MLCCS

As stated in Section II, Fig. 3 only highlights the MLCC behavior at a fixed frequency  $f = 100$  Hz.

It was shown in [9] that the  $E - D$  hysteresis loop of Class II X7R MLCCs does not change its shape for frequencies up to  $f \approx 500$  Hz. Hence, with increasing frequency, the hysteresis loop with associated energy dissipation density  $w$  (see Fig. 2(a)) is cycled more often, such that the dielectric loss density  $\rho$  scales linearly with frequency ( $\alpha = 1.0$ ).

It was found within this study, that this does not apply to Hiteca MLCCs which exhibit an increase in the  $E - D$  hysteresis area  $w$  with increasing frequency. Therefore, for a fixed excitation amplitude the MLCC loss density  $\rho$  increases above-linearly with frequency as presented in Fig. 5(a). However, this loss-frequency behavior can be captured by an iGSEC $_D$  parameter  $\alpha = 1.5$  (see Table 2) which describes the loss density up to 500 Hz (dashed line in Fig. 5(a), (b)) with an error below 20%.

Note that for non-sinusoidal excitation waveforms,  $\alpha \neq 1$  implies that the losses have to be calculated with (7) or (10).

However, the currently employed automated MLCC test setup from [12] does not allow for non-sinusoidal excitation waveforms and it is important to clarify that (7) and (10) have not yet been verified for the Hiteca MLCCs. Future research could extend the MLCC test setup from [12] to allow for arbitrary waveform excitation, and verify (7) and (10) by, e.g., accurately predicting the MLCC losses under third-harmonic injection with increasing third-harmonic amplitude similar to [9], [13].

## REFERENCES

- [1] M. J. Pan and C. Randall, "A brief introduction to ceramic capacitors," *IEEE Elect. Insul. Mag.*, vol. 26, no. 3, pp. 44–50, May–Jun. 2010.
- [2] M. Randall, D. Skamser, J. Kinard, and A. Tajuddin, "Thin film MLCC," in *Proc. Symp. Passive Compon.*, 2007, pp. 372–384.
- [3] K. Syfer, "Syfer application notes," 2014. [Online]. Available: <https://www.digikey.com/en/pdf/k/knownes-syfer/application-notes>
- [4] K. Syfer, "Hiteca range of low loss, high stability Class II capacitors," 2019. [Online]. Available: <https://www.knowlescapacitors.com/getattachment/be4a3a63-0900-4e2d-ae81-f0cc00a2e9f8/Hiteca%E2%84%A2-Multilayer-Ceramic-Capacitors>
- [5] T. Correia, M. Stewart, A. Ellmore, and K. Albertsen, "Lead-free ceramics with high energy density and reduced losses for high temperature applications," *Adv. Eng. Mater.*, vol. 19, no. 6, pp. 1–5, 2017.
- [6] J. Dielectrics, "AC power computations for DC rated capacitors," May 2005. [Online]. Available: <https://www.johansondielectrics.com/downloads/ac-power-computations-for-dc-rated-capacitors.pdf>
- [7] D. Neumayr, D. Bortis, J. W. Kolar, M. Koini, and J. Konrad, "Comprehensive large-signal performance analysis of ceramic capacitors for power pulsation buffers," in *Proc. IEEE 17th Workshop Control Model. Power Electron.*, 2016, pp. 1–8.
- [8] C. B. Barth, T. Foulkes, I. Moon, Y. Lei, S. Qin, and R. C. N. Pilawa-Podgurski, "Experimental evaluation of capacitors for power buffering in single-phase power converters," *IEEE Trans. Power Electron.*, vol. 34, no. 8, pp. 7887–7899, Aug. 2019.
- [9] D. Menzi, D. Bortis, G. Zulauf, M. Heller, and J. W. Kolar, "Novel iGSE-C loss modelling of X7R ceramic capacitors," *IEEE Trans. Power Electron.*, vol. 35, no. 12, pp. 13 367–13 383, Dec. 2020.
- [10] L. E. Mosley, "Capacitor impedance needs for future microprocessors," in *Proc. Symp. Passive Compon.*, 2006, pp. 168–178.
- [11] N. A. Spaldin, "Analogies and differences between ferroelectrics and ferromagnets," in *Proc. Phys. Ferroelect.*, (Topics in Applied Physics Series), 2007, vol. 105, pp. 175–218.
- [12] D. Menzi, M. Heller, and J. W. Kolar, "iGSE-Cx a new normalized steinmetz model for class II multilayer ceramic capacitors," *IEEE Open J. Power Electron.*, vol. 2, pp. 138–144, 2021.
- [13] K. Venkatchalani, C. R. Sullivan, A. Tarek, and T. Hemh, "Accurate prediction of ferrite core loss with nonsinusoidal waveforms using only Steinmetz parameters," in *Proc. IEEE Workshop Comput. Power Electron.*, 2002, pp. 36–41.
- [14] A. Van den Bosche and V. C. Valchev, *Inductors and Transformers Electronics for Power Electronics*. Boca Raton, FL, USA: CRC Press, 2005.
- [15] J. Muhlethaler, J. Biela, J. W. Kolar, and A. Ecklebe, "Core losses under the DC bias condition based on Steinmetz parameters," *IEEE Trans. Power Electron.*, vol. 27, no. 2, pp. 953–963, Feb. 2012.
- [16] J. Xu, L. Gu, and J. Rivas-Davila, "Effect of class 2 ceramic capacitor variations on switched-capacitor and resonant switched-capacitor converters," *IEEE Trans. Emerg. Sel. Topics Power Electron.*, vol. 8, no. 3, pp. 2268–2275, Sep. 2020.
- [17] H. Haag, F. Hämmerle, and S. Ben-Yaakov, "Voltage bias effect on the ESR of ferroelectric ceramic capacitors," in *Proc. IEEE Power Convers. Intell. Motion Conf.*, 2020, pp. 1–6.
- [18] A. Tyshko and S. Balevicus, "Specifics of the X7R capacitors application in the high frequency inverters," in *Proc. IEEE 36th Int. Conf. Electron. Nanotechnol.*, 2016, pp. 267–270.
- [19] S. Coday and R. C. N. Pilawa-Podgurski, "High accuracy calorimetric measurements and modeling of ceramic capacitor losses under large ripple operation," in *Proc. IEEE Appl. Power Electron. Conf.*, 2020, pp. 188–194.
- [20] J. M. Ingman et al., "Localization of dielectric breakdown defects in multilayer ceramic capacitors using 3D x-ray imaging," *J. Eur. Ceram. Soc.*, vol. 39, no. 4, pp. 1178–1185, Apr. 2019.
- [21] Y. Jiang, B. Hu, B. Wen, Y. Shen, and T. Long, "Loss characterization and modeling of ferroelectric class II multi-layer ceramic capacitors in resonant converters," Dec. 2022. [Online]. Available: <https://www.doi.org/10.36227/techrxiv.21741359.v1>



**DAVID MENZI** (Member, IEEE) received the B.Sc. and M.Sc. degrees in electrical engineering and information technology from the Swiss Federal Institute of Technology (ETH), Zurich, Switzerland, in 2015 and 2017, respectively, where he focused on power electronics, control theory, and high voltage technology. He also spent a semester with the Royal Institute of Technology (KTH), Stockholm, Sweden as an Exchange Student. During his studies, he was with ABB Medium Voltage Drives (MVD), Turgi, Switzerland, as an Intern

and Working Student. He conducted his Ph.D. research in electrical engineering from 2018 to 2022 on bidirectional phase-modular three-phase buck-boost converter systems under the supervision of Prof. J.W. Kolar at the Power Electronic Systems Laboratory (PES) of ETH Zurich, where he is currently working as a Postdoctoral Researcher.



**MORRIS HELLER** (Student Member, IEEE) received the B.Sc. degree in electric engineering from Hochschule Luzern/FHZZ, Luzern, Switzerland, in 2014, and the M.Sc. degree in electrical engineering and information technology, with a focus on power electronic systems design and power semiconductor technology, from ETH Zurich, Zurich, Switzerland, in 2018, where he also conducted his Ph.D. research with the Power Electronic Systems Laboratory, and received the Ph.D. degree with a focus on three-phase PFC rectifiers

and multi-port power converters in 2023.



**GEORGE KERRIDGE** received the M.Eng. and Ph.D. degrees in materials science and engineering from the University of Sheffield, Sheffield, U.K., in 2016 and 2021, respectively. His Ph.D. was in functional ceramics research, with a focus on predicting and developing novel composite material systems for multilayer ceramic capacitor applications. This work resulted in a 1st author paper, published in 2021. Since 2022, he has been a Junior Research and Development Engineer of Knowles Precision Devices, working on the various types of

capacitors and other products.



**PETER MARLEY** received the B.A. degree in chemistry from Alfred University, Alfred, NY, USA, and the Ph.D. degree in chemistry from the University of Buffalo, Buffalo, NY, USA, in 2015 with a focus on structure-property relationships in electronic ceramic nanomaterials. He is currently a Senior Scientist of ceramics R&D and knowles precision devices. He authored or coauthored more than 20 papers with multiple patents filed on the topic of electronic ceramics and the resulting performance. More than seven years of

industry experience developing novel electronic dielectric ceramics for capacitor and filter technologies.



**ANGELA ELLMORE** is currently the Global Director of R&D – Capacitors, Knowles Precision Devices. She is/was a Fellow of the Royal Society of Chemistry and Chartered Chemist. She has more than 40 years of experience with the MLCC Industry. She managed the Process Engineering Department and R&D for the Syfer brand when manufactured in the U.K., specialising mainly in material engineering., and transitioned to a Global R&D Leadership role about seven years ago. She launched numerous new products, some with asso-

ciated patent protection.



**SHMUEL (SAM) BEN-YAAKOV** (Life Fellow, IEEE) received the B.Sc. degree in electrical engineering from the Technion, Haifa, Israel, in 1961, and the M.Sc. and Ph.D. degrees in engineering from the University of California, Los Angeles, CA, USA, in 1967 and 1970, respectively. He is currently a Professor Emeritus with the Department of Electrical and Computer Engineering, Ben-Gurion University of the Negev, Beer-Sheva, Israel. During 1985–1989, he was the Chairman of the Department of Electrical and Computer Engi-

neering, Ben-Gurion University. In 1984, he established the Power Electronics Laboratory, Ben-Gurion University (PEL-BGU), as a Center of knowledge and excellence in analog and power electronics. He started and currently cultivates the YouTube's Sam Ben-Yaakov channel in which he is posting educational videos (<https://www.youtube.com/user/sambenyaakov/videos>). His research interests include analog and power electronics, and engineering education. Professor Ben-Yaakov is a Consultant to commercial companies and governmental agencies worldwide and was an Entrepreneur and the Founder of start-up companies. He is also the Chief Innovation Officer of IRP Systems, Ness Ziona Science Park, Israel (<https://www.irpsystems.com/>) - managing the research and development of advanced technologies in the area of EV power train.



**JOHANN W. KOLAR** (Fellow, IEEE) received the M.Sc. and Ph.D. degree (*summa cum laude*) from the University of Technology Vienna, Vienna, Austria, in 1997 and 1999, respectively. Since 1984, he has been working as an independent Researcher and International Consultant of close collaboration with the Vienna University of Technology in the fields of power electronics, industrial electronics and high performance drive systems. He was appointed Assoc. Professor and the Head of the Power Electronic Systems Laboratory, Swiss Fed-

eral Institute of Technology (ETH) Zurich, Zurich, Switzerland, in February 1, 2001, and was promoted to the rank of Full Professor in 2004. Dr. Kolar has proposed numerous novel converter concepts include the Vienna Rectifier, Sparse Matrix Converter, and Swiss Rectifier, has spearheaded the development of x-million rpm motors, and has pioneered fully automated multi-objective power electronics design procedures. He has graduated more than 80 Ph.D. students, has authored or coauthored more than 1000 journal and conference papers and four book chapters, and has filed more than 200 patents in the course of international industry research collaborations. He has presented more than 40 educational seminars at leading international conferences and was IEEE PELS Distinguished Lecturer during 2012 – 2016. His research interests include ultracompact/efficient WBG converter systems, ANN-based design procedures, solid-state transformers, ultra-high speed drives, bearingless motors, and life cycle analysis of power electronics converter systems. He was the recipient of more than 40 IEEE Transactions and Conference Prize Paper awards, 2014 IEEE Power Electronics Society R. David Middlebrook Achievement Award, 2016 IEEE PEMC Council Award, 2016 IEEE William E. Newell Power Electronics Award, 2021 EPE Outstanding Achievement Award, and two ETH Zurich Golden Owl awards for excellence in teaching. He was elected to the U.S. National Academy of Engineering as an International Member in 2021.